New Class of Bioinspired Lenses with a Gradient Refractive Index

Y. Jin,[1] H. Tai,[1*] A. Hiltner,[1] E. Baer,[1] James S. Shirk[2]

[1]*Department of Macromolecular Science and Center for Applied Polymer Research, Case Western Reserve University, Cleveland, Ohio 44106-7202*
[2]*Optical Sciences Division, Naval Research Laboratory, Washington, DC 20375*

Received 15 July 2006; accepted 10 August 2006
DOI 10.1002/app.25404
Published online in Wiley InterScience (www.interscience.wiley.com).

ABSTRACT: The recognition that eye lenses in nature often employ a gradient refractive index to enhance the focusing power and to correct aberrations has motivated us to construct a synthetic lens using the layered concept encountered in biological lenses. The result is a highly flexible technology for the fabrication of gradient-refractive index lenses that is based on a method of polymer forced assembly. Polymeric nanolayered films with incremental differences in the refractive index are assembled according to a prescribed design and molded into the desired shape. The exceptional flexibility of the process lies in the wide range of lens shapes and index profiles that can be realized. A lens with any refractive index distribution can be achieved within the refractive index range of available coextrudable optical materials.
 J Appl Polym Sci 103: 1834–1841, 2007

Key words: nanolayers; coextrusion; biomimetic; gradient refractive index

INTRODUCTION

Gradient refractive index (GRIN) materials have the potential to vastly simplify the design of high-quality optical systems. Biological lenses often use a gradient index to enhance the focusing power and to correct aberrations.[1–4] The refractive index range (Δn) of a human eye lens is about 0.03.[5] Δn of the octopus eye is about 0.15,[6] and Δn of the fish eye is about 0.22.[7] In the fish eye and the octopus eye, which function in water, the optical power is almost entirely derived from the high value of Δn. Because the octopus has no cornea and the refractive index of the lens is close to that of sea water, the nearly parabolic GRIN distribution in the spherical lens provides all the focusing power of its eye.[8]

The utility of index gradients for optical devices is well known.[9,10] There is substantial literature describing efforts to fabricate optical materials with a gradient index from inorganic glasses or optically transparent polymers.[11] For polymers, these include diffusion copolymerization,[12–14] extrusion copolymerization,[15–17] plasma copolymerization,[18,19] interfacial gel copolymerization,[20–25] variations of the interfacial gel method,[26] photocopolymerization,[27,28] and centrifugal diffusing polymerization.[29,30] Spherical GRIN lenses have been reported by suspension polymerization.[31,32] In these processes, the index gradient is formed by diffusion. The gradients are typically limited to low Δn values (<0.05) and an inflexible GRIN distribution.

Biological GRIN lenses consist of layered assemblies. Systematic variation in the protein and water concentration provides the index gradient.[33] The human lens has approximately 22,000 layers.[34] Inspired by this biological design, we developed a new class of synthetic lenses with controlled GRIN distributions by assembling polymeric nanolayered films.

In contrast to the well-known concept of self-assembly, layer-multiplying coextrusion uses forced assembly to create thousands of alternating layers of two polymers.[35] Individual layers can be less than 10 nm thick.[36,37] The reflective characteristics of polymer forced assemblies are exploited to fabricate films with colorful iridescence,[38] with narrow band transmission (one-dimensional photonic crystals),[39] or with other optical properties.[40] However, if the layers are thinner than a quarter wavelength ($\lambda/4n$), they are transparent, and the refractive index is effectively an average of those of the constituent materials. This article describes the utilization of polymeric nanolayer assemblies in the construction of synthetic GRIN materials.

EXPERIMENTAL

The polymers used in the construction of the GRINS lens were polycarbonate (PC) with a refractive index of 1.58 (Calibre 200-10, Dow Chemical Co., Midland, MI), poly(methyl methacrylate) (PMMA) with a refractive index of 1.49 (Plexiglas V826, Atofina Chemicals, Inc., Geneseo, NY), and a styrene–acrylonitrile copolymer

**Present address:* 3M, Minneapolis, MN.
Correspondence to: A. Hiltner (ahiltner@case.edu).
Contract grant sponsor: National Science Foundation; contract grant number: DMR-0349436.
Contract grant sponsor: Defense Advanced Research Projects Agency; contract grant number: HR0011-04-C-0043.

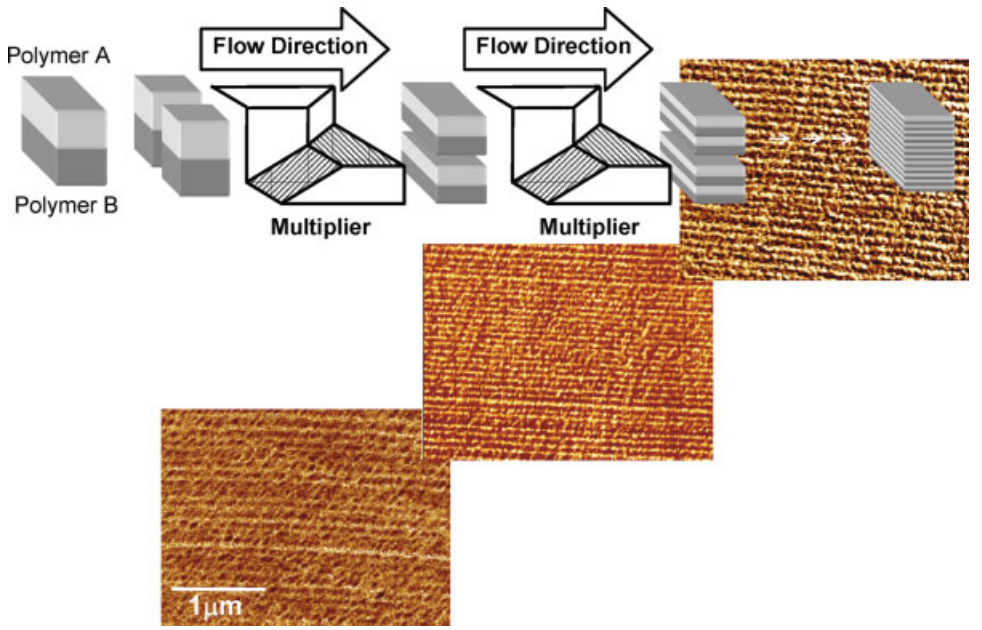

Figure 1 AFM phase images showing three PC/PMMA nanolayer films with compositions of 30/70, 50/50, and 70/30. The light layers are PC, and the dark layers are PMMA. [Color figure can be viewed in the online issue, which is available at www.interscience.wiley.com.]

with 17 wt % acrylonitrile (SAN17) with a refractive index of 1.57 (Lustran, Bayer AG, Pittsburgh, PA). In addition, poly(vinylidene fluoride-*co*-trifluoroethylene) (PVDF) with a refractive index of 1.40 (Solef 21508, Solvay Plastics, Alpharetta, GA) was blended with PMMA in a 1 : 1 (w/w) composition at 230°C with a twin-screw extruder (PVDF-blend). The PVDF-blend had a refractive index of 1.45.

Nanolayer films with 2048 alternating layers of PC/PMMA, SAN17/PMMA, and PMMA/PVDF-blend were extruded from the melt on a laboratory-scale coextrusion line at Case Western Reserve University that incorporated the layer-multiplying technology.[35] The extruder temperatures were adjusted to ensure that the viscosities matched when the melts were combined in the feed block. From the feed block, the melt stream flowed through a series of layer-multiplying die elements (Fig. 1). Each element split the melt vertically, spread it horizontally, and finally recombined it with twice the number of layers. An assembly of n multipliers produced a film with 2^{n+1} layers. The films used to fabricate the GRIN lenses were extruded with 10 multipliers to give films with 2048 layers. The 50-μm-thick films were extruded onto a chill roll with a take-off speed of 15 feet/min. Thus, the thickness of individual layers in a 50/50 (v/v) film was about 25 nm. Some 12-μm-thick films were also extruded. The film composition ratio (v/v) was varied by the careful control of the feed rates with metering pumps.

The layered structure was examined with atomic force microscopy (AFM). The film was embedded in epoxy (SPI-Chem/SPI-PON 812 KIT formulation, SPI Supplies Division, Structure Probe, Inc., West Chester, PA) and cured for 8 h at 60°C. The cross sections were microtomed perpendicularly to the plane of the film and observed directly. The AFM images were obtained in air with a commercial scanning probe microscope (Nanoscope IIIa, Digital Instruments, Santa Barbara, CA) operated in the tapping mode. The measurements were performed under ambient conditions with rectangular Si probes with a spring constant of 50 N/m and a resonance frequency in the 284–362-kHz range. The tip radius was 10 nm.

Attenuated total reflectance/Fourier transform infrared (ATR–FTIR) microspectroscopy data were collected with a Nexus 870 Fourier transform infrared bench coupled to a Continuum microscope (Thermo Nicolet, Madison, WI). The microscope used an attenuated-total-reflectance slide-on attachment with a germanium crystal to allow attenuated-total-reflectance microanalysis. Spectra were collected at a resolution of 2 cm^{-1} for 32 scans. Each spectrum sampled an area of 75 μm × 75 μm. Individual spectra were collected at 320-μm intervals over the lens surface for GRIN lenses 20 mm in diameter, at 120-μm intervals for GRIN lenses 6 mm in diameter, and at 60-μm intervals for GRIN lenses 3 mm in diameter. To determine the refractive index gradient along the z direction through the center of the lens, the SAN17/PMMA lens was embedded in epoxy and cut through the center.

RESULTS AND DISCUSSION

A series of nanolayered films that differed in the refractive index by about 0.0009 was produced by the systematic variation of the constituent ratios during coex-

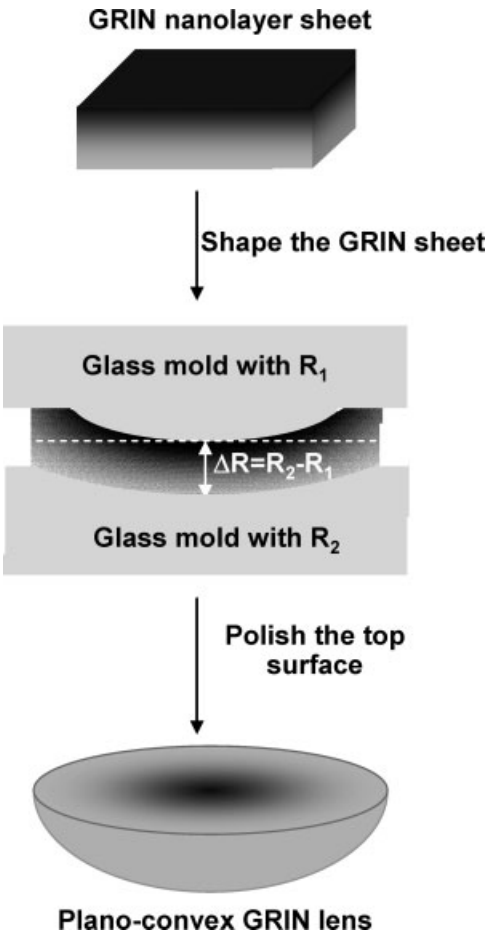

Figure 2 Schematic drawings illustrating the process by which a consolidated GRIN stack of nanolayer films is shaped and polished into a plano–convex GRIN lens.

trusion. The AFM phase images in Figure 1 show three compositions from the 101 films that combined PC ($n =$ 1.58) and PMMA ($n = 1.49$). The variation in the composition is evident from the relative layer thicknesses. The observed refractive index of the films varied linearly with the composition (relative layer thickness), as expected from effective medium theory. Δn was 0.09 for nanolayered films of PC and PMMA. Films that combined SAN17 with PMMA had a Δn value of 0.08. A higher Δn value of 0.12 was obtained by the joining of SAN17/PMMA films and films that combined PMMA with PVDF-blend. Lenses fabricated from the joined SAN17/PMMA and PMMA/PVDF-blend films are identified as SAN17/PVDF-blend lenses.

A clear, thick sheet with a specific refractive index gradient was constructed by the stacking of nanolayered films of different compositions. To minimize the birefringence of the GRIN sheet, each film was rotated randomly when stacking. By the appropriate choice of the composition of each film, it was possible to produce a sheet with any refractive index distribution within Δn of the constituent polymers. Sequentially stacking a single film of each of the 101 50-μm-thick SAN17/PMMA compositions produced a sheet about 5 mm thick with a linear refractive index gradient with a Δn value of 0.08. The stack was consolidated with a thickness reduction to about 4 mm in a compression molder at 130°C under high pressure. The consolidated sheet contained more than 20,000 nanolayers, a number comparable to the number of layers in the human lens.

The GRIN lens was fabricated by the placement of the GRIN sheet between a concave, spherical mold with radius R_2 of 23.5 mm and a convex, spherical mold with radius R_1 of 20.7 mm, with the higher refractive index side of the sheet against the convex mold, as shown schematically in Figure 2. Slight pressure at 130°C shaped the sheet into a spherical shell having the radii of the molds. A spacer was used to ensure that the separation of the molds would be equal to the difference, $\Delta R = R_2 - R_1$ or 2.8 mm. The GRIN distribution of the sheet was preserved in the shaped, spherical shell. After shaping, the concave surface of the GRIN shell was polished to optical smoothness to obtain a plano–convex GRIN lens (Fig. 3). The final lens diameter was typically 15 mm.

The shaped GRIN sheet is part of the large, imaginary GRIN sphere shown in Figure 4, with the parabolic radial index distribution, $N(R)$, given as follows:

$$N(R) = N_0\left(1 - \frac{AR^2}{2}\right) \quad (1)$$

where R is the distance from the center of the sphere and N_0 is the refractive index at the center of the sphere

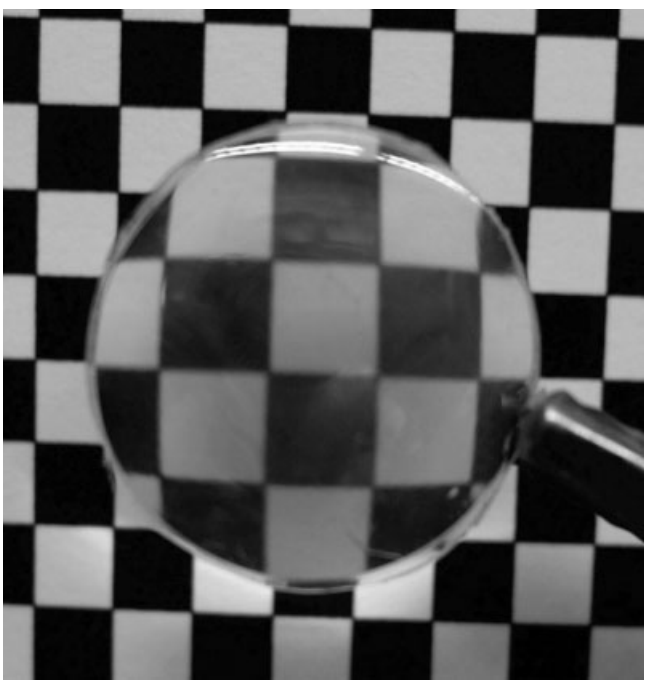

Figure 3 Checkerboard pattern magnified through a 20-mm plane–convex SAN17/PMMA GRIN lens that contains tens of thousands of polymer layers.

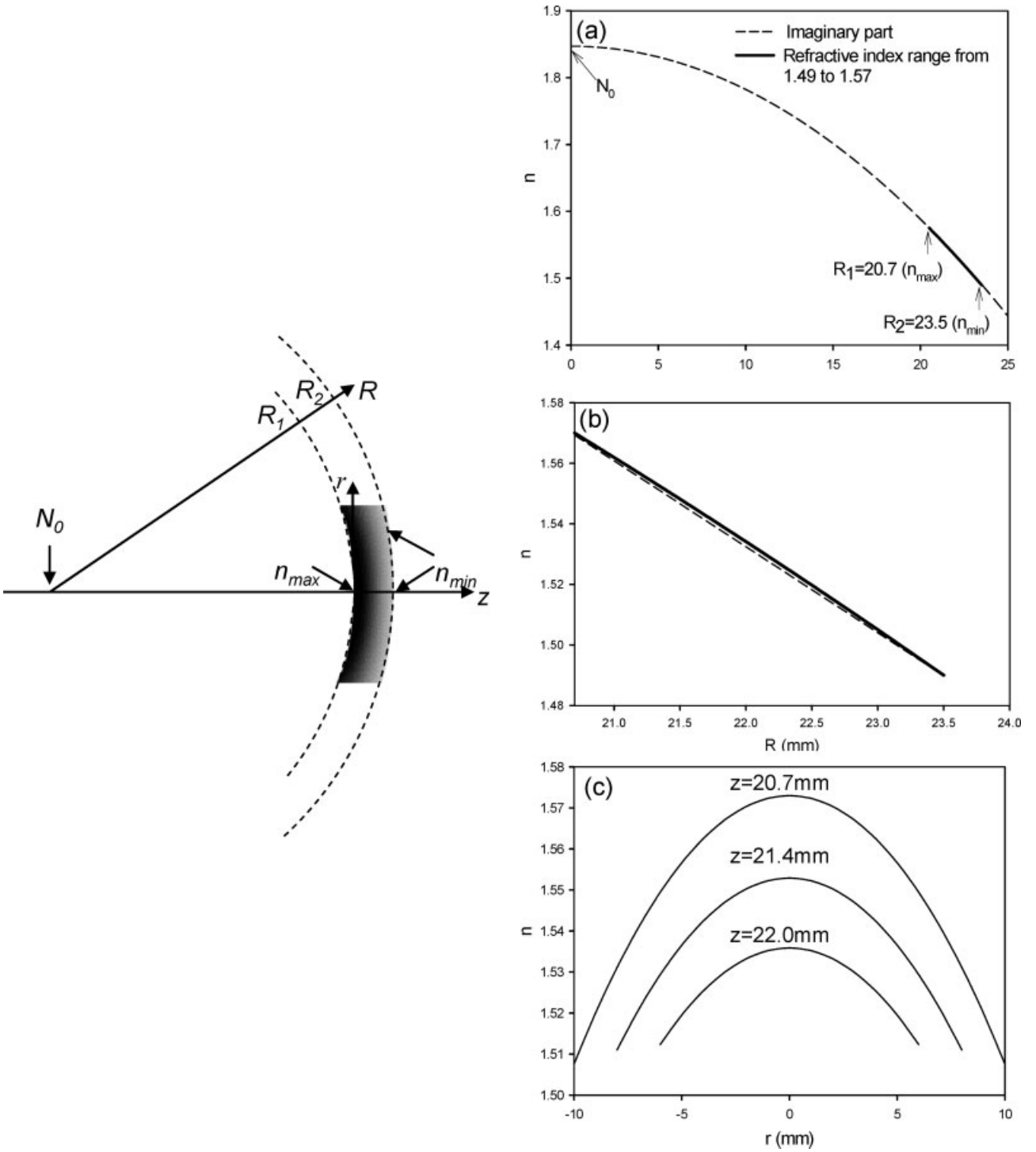

Figure 4 Shaped GRIN sheet as part of a large, imaginary GRIN sphere: (a) the parabolic radial GRIN distribution of the imaginary GRIN sphere, (b) the almost linear GRIN distribution in the region of the fabricated GRIN lens, and (c) the parabolic refractive index gradient on planes perpendicular to the optical axis at distance z from the center of the imaginary GRIN sphere.

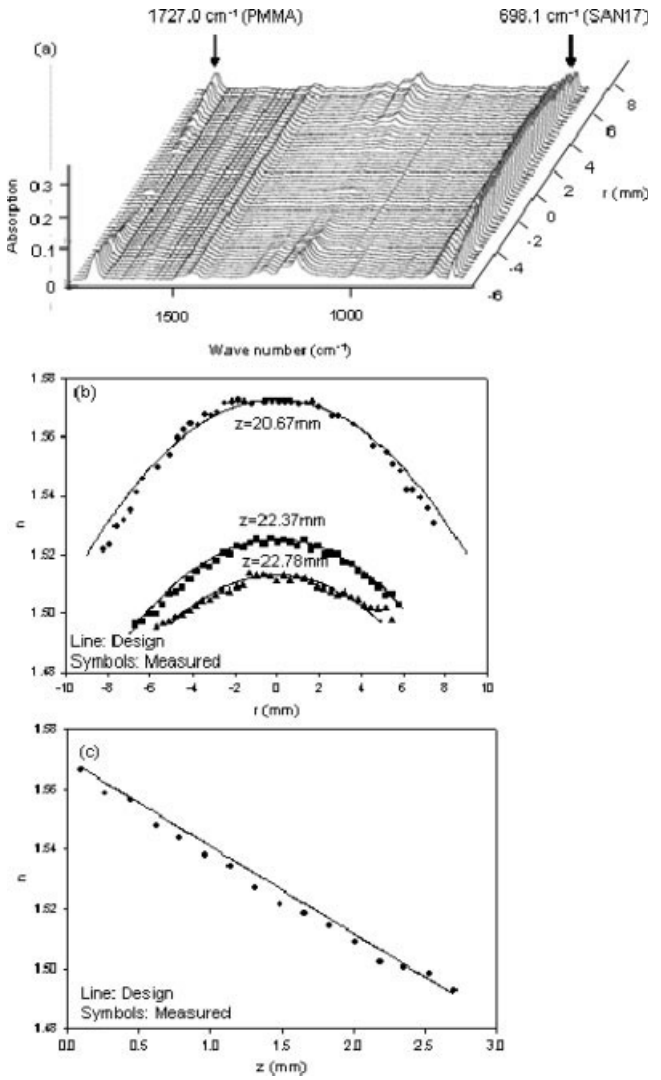

Figure 5 Refractive index gradient on the plane surface obtained by the measurement of the composition at various positions with ATR–FTIR microspectroscopy: (a) a series of spectra collected across the diameter of the plano surface of a SAN17/PMMA GRIN lens, (b) a comparison of the plano refractive index gradient from the composition with the parabolic refractive index gradient predicted by the lens design at various positions through the thickness of the lens, and (c) a comparison of the refractive index gradient from the composition with the linear refractive index gradient predicted by the lens design along the optical axis.

and A is a constant. If the spherical shell has n_{max} at R_1 and n_{min} at R_2, N_0, and A can be obtained as follows:

$$N_0 = \frac{n_{max}R_2^2 - n_{min}R_1^2}{R_2^2 - R_1^2} \quad (2)$$

$$A = \frac{2(n_{max} - n_{min})}{n_{max}R_2^2 - n_{min}R_1^2} \quad (3)$$

For a SAN17/PMMA shell with $n_{max} = 1.57$ at $R_1 = 20.7$ and $n_{min} = 1.49$ at $R_2 = 23.5$, N_0 is 1.85 and A is 7.06×10^{-4} mm^{-2}. In the region of the fabricated GRIN lens, the parabolic refractive index distribution is very close to linear. Thus, a linear GRIN sheet can be used to fabricate the plano–convex GRIN lens to a very good approximation.

The polished surface of the GRIN lens is a plane perpendicular to the radius at distance z from the center of the imaginary sphere. The refractive index on the plano surface at any distance r from the optical axis is given as follows:

$$n(r) = n_0\left(1 - \frac{a(r^2)}{2}\right) \quad (4)$$

where n_0 is the refractive index at the center of the plane

$$n_0 = N_0\left(1 - \frac{Az^2}{2}\right) \quad (5)$$

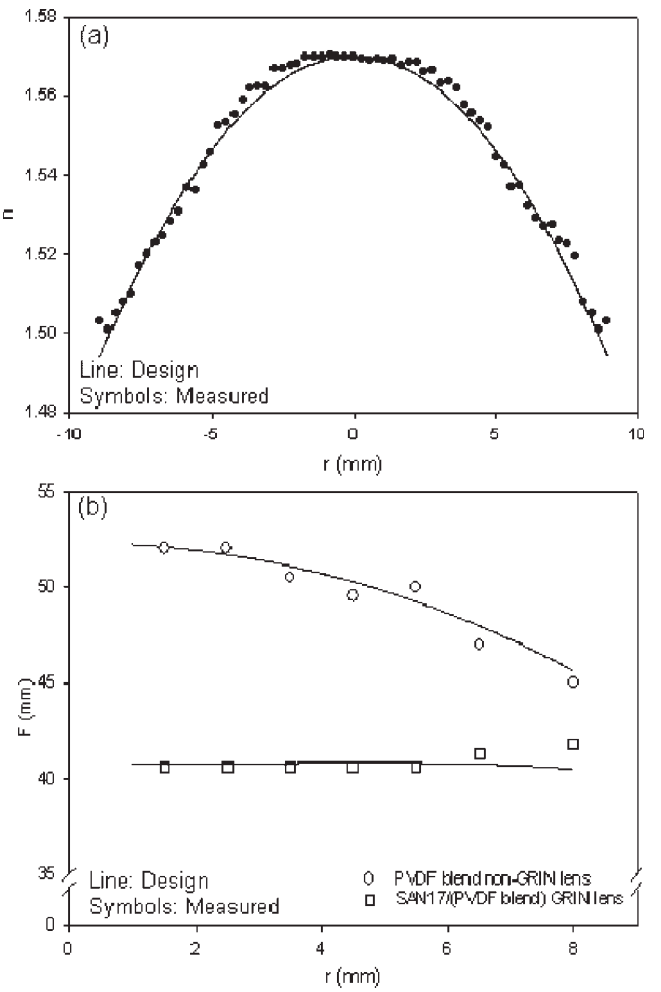

Figure 6 The GRIN component largely compensates for the spherical aberration from the curved surface of the plano–convex lens: (a) the GRIN distribution on the plano surface of a SAN17/PVDF-blend GRIN lens and (b) the focal length measured at various positions compared with the focal length of a non-GRIN PVDF blend lens with the same shape as the GRIN lens.

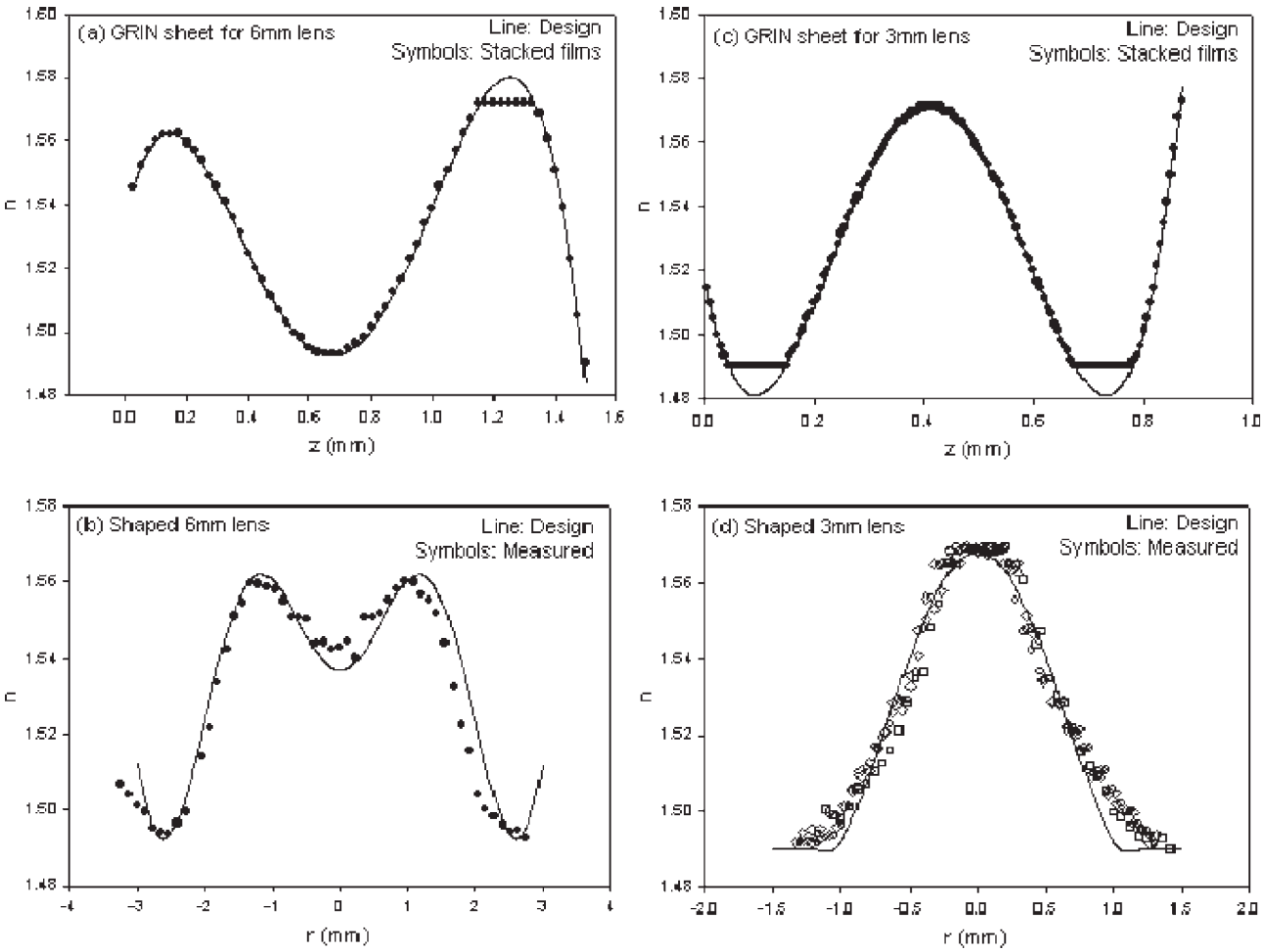

Figure 7 The flexibility of the bioinspired approach lies in the wide variety of index gradients that are possible in a GRIN sheet. (a) The prescribed index distribution of a GRIN sheet (solid line) is shown for (b) the target plano distribution of a 6-mm plano–convex lens. The sixty 50-μm-thick SAN17/PMMA films that were assembled into the GRIN sheet are identified by solid points in part a, and the resulting plano GRIN distribution after the sheet was shaped between a convex mold with $R_2 = 4.74$ mm and a concave mold with $R_1 = 6.20$ mm and was polished is described by the solid points in part b. (c) The prescribed index distribution of a GRIN sheet (solid line) is shown for (d) the target plano distribution of a 3-mm plano–convex lens. The 139 13-μm-thick SAN17/PMMA films that were assembled into the GRIN sheet are identified by solid points in part c, and the resulting plano GRIN distribution after the sheet was shaped between a convex mold with $R_2 = 6.20$ mm and a concave mold with $R_1 = 7.06$ mm and was polished is described by the solid points in part d.

and a is given as

$$a = A\left(1 - \frac{Az^2}{2}\right)^{-1} \tag{6}$$

The refractive index gradient on the plano surface of the GRIN lens is obtained by the measurement of the composition at various positions by ATR–FTIR microspectroscopy. A series of spectra collected across the diameter of the plano surface ($z = 20.7$ mm) of the SAN17/PMMA GRIN lens are included in Figure 5. The composition is determined from the normalized intensity of the characteristic peaks for SAN17 at 698 cm^{-1} and for PMMA at 1727 cm^{-1}. The refractive index is calculated from the composition of the effective medium composite. The parabolic refractive index gradient is confirmed for other planes perpendicular to the optical axis by the systematic reduction of the thickness of the lens with further polishing. The linear distribution through the lens along the optical axis can be approximated as follows:

$$n(z) = n_{max} - \left(\frac{z - R_1}{R_2 - R_1}\right)(n_{max} - n_{min}) \tag{7}$$

This can be confirmed by microspectroscopy.

The focal length (F) of the plano–convex GRIN lens depends on the combined effects of the GRIN and the lens curvature. Normally, the optical performance would be determined by means of ray tracing. However, a simple closed solution exists for the focusing power of a flat GRIN medium with a radial parabolic refractive index gradient,[41] and the GRIN contribution of the plano–convex lens can be obtained analyti-

cally. The contribution of the lens curvature to the focusing power is readily obtained from geometric optics and Snell's refraction law. The summation of the two contributions gives

$$\frac{1}{F} = \frac{2(n_{\max} - n_{\min})}{R_2^2 - R_1^2}\left(\sqrt{R_2^2 - r^2} - R_1\right) + \left(\sqrt{R_2^2 - r^2} + \frac{r}{\tan\left(\arcsin(\frac{r}{R_2} \cdot \frac{n_{\min}}{n_{air}}) - \arcsin(\frac{r}{R_2})\right)} - R_2\right)^{-1}$$

where n_{air} is the refractive index of air.

The on-axis F value is measured with a simple two-pinhole approach:

$$F = \frac{ld_1}{d_1 + d_2} \tag{9}$$

where d_1 is the pinhole separation of two incident collimated laser beams with a wavelength of 633 nm, d_2 is the separation of the laser spots projected on a screen behind the lens, and l is the distance from the lens to the screen. The dependence of F on r of a SAN17/PVDF-blend GRIN lens with the plane index distribution in Figure 6(a) and a non-GRIN PVDF blend lens with the same shape as the GRIN lens are compared in Figure 6(b). The GRIN component shortens F and largely compensates for the spherical aberration from the curved surface, as evidenced by the flat dependence of F on r.

The flexibility of the bioinspired approach lies in the wide variety of index gradients that are possible in the GRIN sheet and in the almost unlimited range of shapes that can be molded. By the appropriate choice of the composition of each film, it is possible to produce a sheet with any refractive index distribution within Δn of the constituent polymers. Ray tracing is used to determine the specific index distribution and the required mold geometry to achieve a particular lens design. The distribution given by the solid line in Figure 7(a) is prescribed for a small 6-mm plano–convex GRIN lens, with the target plano distribution given by the solid line in Figure 7(b). To realize the design, SAN17/PMMA films were stacked in the sequence described by the solid points in Figure 7(a). After the stack was shaped and polished into a plano–convex lens, the plano distribution closely replicated the design in Figure 7(b).

A smaller 3-mm GRIN lens was molded from a GRIN sheet described in Figure 7(c). The target index distribution given by the solid line was mimicked by a stack of SAN17/PMMA films identified by the solid points. The stack was shaped and polished to obtain a plano–convex lens with the target plano GRIN distribution in Figure 7(d). Measurements along three diameters demonstrate the uniformity of the plano GRIN distribution. Further development of ray-tracing techniques can enable the design of synthetic optical systems that have fewer, lighter lenses than traditional systems.

CONCLUSIONS

A new class of bioinspired optical materials has been described. Like biological lenses, the new lenses incorporate both a nanolayered structure and a refractive index gradient. The assembly of many layers with gradual changes in the refractive index is enabled by layer-multiplying coextrusion. A typical lens assembly incorporates 20,000 individual nanolayers, comparable to the number of protein layers in the human lens. Any refractive index distribution can be achieved within Δn of available coextrudable optical materials.

The authors thank Marie Sandrock and Michael Wiggins of the Naval Research Laboratory for many stimulating discussions.

References

1. Gullstrand, A. In Helmholtz's Treatise on Physiological Optics; Southall, J. P. C., Ed.; Optical Society of America: Washington, DC, 1924.
2. Atchison, D. A.; Smith, G. Vision Res 1995, 35, 2529.
3. Moffat, B. A.; Atchison, D. A.; Pope, J. M. Vision Res 2002, 42, 1683.
4. Gardneer, L. F.; Smith, G.; Yao, S.; Augusteyn, R. C. Vision Res 2001, 41, 973.
5. Berrgman, L.; Schaefer, C. Optics of Waves and Particles; de Gruyter: New York, 1999.
6. Jagger, W. S.; Sands, P. J. Vision Res 1999, 39, 2841.
7. Jagger, W. S.; Sands, P. J. Vision Res 1996, 36, 2623.
8. Mutti, D. O.; Zadnik, K.; Adams, A. J. Vision Res 1995, 35, 1565.
9. Moore, D. T. Appl Opt 1980, 19, 1035.
10. Gordon, J. M. Appl Opt 2000, 39, 3825.
11. Kitano, I.; Koizumi, K.; Matsumura, H.; Uchida, T.; Furukawa, M. J Jpn Soc Appl Phys 1970, 39, 63.
12. Ohtsuka, Y.; Terao, Y. J Appl Polym Sci 1981, 26, 2907.
13. Ohtsuka, Y.; Sugano, T. Appl Opt 1983, 22, 413.
14. Wu, S. P.; Nihei, E.; Koike, Y. Appl Opt 1996, 35, 28.
15. Ho, B. C.; Chen, J. H.; Chen, W. C.; Chang, Y. H.; Yang, S. Y.; Chen, J. J.; Tseng, T. W. Polym J (Tokyo) 1995, 27, 310.
16. Chen, W. C.; Chen, J. H.; Yang, S. Y.; Cherng, J. Y.; Chang, Y. H.; Ho, B. C. J Appl Polym Sci 1996, 60, 1379.
17. Hsu, J. H.; Lin, S. H. Polymer 2003, 44, 5461.
18. Beltrami, D. R.; Love, J. D.; Durandet, A.; Samoc, A.; Samoc, M.; Luther-Davies, B.; Boswell, R. W. Electron Lett 1996, 32, 549.
19. Jiang, H.; O'Neill, K.; Grant, J. T.; Tullis, S.; Eyink, K.; Johnson, W. E.; Fleitz, P.; Bunning, T. J. Chem Mater 2004, 16, 1292.
20. Liu, J. H.; Liu, H. T. Opt Lett 1997, 22, 668.
21. Liu, J. H.; Liu, H. T. Polymer 1997, 38, 1251.
22. Liu, J. H.; Liu, H. T.; Cheng, Y. B. Polymer 1998, 39, 5549.
23. Koike, Y.; Takezawa, Y.; Ohtsuka, Y. Appl Opt 1988, 27, 486.
24. Koike, Y.; Nihei, E.; Tanio, N.; Ohtsuka, Y. Appl Opt 1990, 29, 2686.
25. Wang, D. J.; Gu, C. B.; Chen, P. L.; Liu, S. X.; Zhen, Z.; Zhang, J. C.; Liu, X. H. J Appl Polym Sci 2003, 87, 280.
26. Masere, J.; Lewis, L. L.; Pojman, J. A. J Appl Polym Sci 2001, 80, 686.

27. Koike, Y.; Kimoto, Y.; Ohtsuka, Y. Appl Opt 1982, 21, 1057.
28. Liu, J. H.; Wang, J. H.; Chu, M. H. Angew Makromol Chem 1990, 174, 1.
29. Liu, J. H.; Chen, J. L.; Wang, H. Y.; Tsai, F. R. Macromol Chem Phys 2000, 201, 126.
30. Liu, J. H.; Wu, D. S.; Tseng, K. Y. Macromol Chem Phys 2004, 205, 2205.
31. Koike, Y.; Sumi, Y.; Ohtsuka, Y. Appl Opt 1986, 25, 3356.
32. Koike, Y.; Kanemitsu, A.; Shioda, Y.; Nihei, E.; Ohtsuka, Y. Appl Opt 1994, 33, 3394.
33. Walls, G. L. The Vertebrate Eye and Its Adaptive Radiation; Hafner: New York, 1963.
34. Bergmann, L.; Schaefer, C. Optics of Waves and Particles; de Gruyter: New York, 1999.
35. Mueller, C. D.; Nazarenko, S.; Ebeling, T.; Schuman, T.; Hiltner, A.; Baer, E. Polym Eng Sci 1997, 37, 355.
36. Kerns, J.; Hsieh, A.; Hiltner, A.; Baer, E. J Appl Polym Sci 2000, 77, 1545.
37. Mueller, C.; Topolkaraev, V.; Soerens, D.; Hiltner, A.; Baer, E. J Appl Polym Sci 2000, 78, 816.
38. Alfrey, T., Jr.; Gurnee, E. F.; Schrenk, W. J. Polym Eng Sci 1969, 9, 400.
39. Tangirala, R.; Baer, E.; Hiltner, A.; Weder, C. Adv Funct Mater 2004, 14, 595.
40. Weber, M. F.; Stover, C. A.; Gilbert, L. R.; Nevitt, T. J.; Ouderkirk, A. J. Science 2000, 287, 2451.
41. Gomez-Reino, C.; Perez, M. V.; Bao, C. Gradient-Index Optics Fundamentals and Applications; Springer-Verlag: Berlin, 2002.